Dynamical properties of a model for synchro-betatron coupling

L. Bongini*, G. Franchetti**, G. Turchetti *

* *Dip. di Fisica and INFN Bologna, ITALY .*
** *GSI, Darmstadt, Germany*

Abstract The long term stability of betatron motion in presence of multipolar nonlinearities has been extensively investigated for high energy accelerators and the Hénon maps has been proposed as a model. In high intensity accelerators the non linear effects due to space charge and synchro-betatron coupling are relevant. We propose a simple model to investigate the coupling between longitudinal and horizontal motion due to chromaticity. The model consists in a standard Chirikov map coupled to a Hénon map. Diffusion of orbits is observed and the structure of resonances is inspected by the frequency analysis.

INTRODUCTION

High intensity beams are facing new applications beyond basic research in nuclear physics [1,2]. In the absence of space charge the multipolar errors and the cavities exert nonlinear forces on the transverse and longitudinal motion. The space charge force has a defocusing effect on the transverse motion and couples it to the longitudinal one. A synchro-betatron coupling occurs also because any change of momentum displaces the closed orbit and in presence of sextupoles or higher multipoles the tune changes (chromatic effect).
To investigate the coupling we propose a simple 4D model consisting in a standard map which describes the effect of a thin RF cavity and a 2D Hénon map which describes the effect of a thin sextupole for a flat beam. We make the linear tune vary with the longitudinal momentum and require the map to be symplectic. This fixes the longitudinal displacement due to the coupling with the transversal motion. When a particle is almost synchronous and near to the corresponding close orbit, the coupling effect is negligible. For large transverse displacements the coupling with the longitudinal motion becomes visible when a large island is encountered, because the frequency is slowly modulated and adiabatic invari-

ance is lost close to the islands border, where a localized diffusion is observed. When the particle approaches the borderline of the bucket, namely the pendulum separatrix, the diffusion in the transverse phase plane is enhanced. A similar diffusion pattern occurs for a Hénon map whose linear frequency is stochastically perturbed. The frequency analysis and the tune-action map provide the global pattern of the resonances and of the chaotic regions.

THE SYNCHRO-BETATRON MAP

The design of high energy accelerators like LHC requires a stable beam on a high number turns ($\sim 10^8$ corresponding to 10^{11} crossings of FODO cells). As a consequence the dynamic aperture and the ripple induced diffusion in presence of multipolar errors have been actively investigated [3,4]. In the case of a high intensity LINAC [1] the number of FODO cells does not exceed 10^3 whereas the storage ring of HIDIF [2] has 10^2 cells visited during 10^2 turns. Since the number of FODO crossings does not exceed 10^4 we are not very concerned with the long term stability and only the short term dynamic aperture is relevant. It is well known that a particle with momentum p different from the design momentum p_s follows a different closed orbits and its linear tune is shifted by $\alpha\,(p-p_s)/p_s$. This tune shift may be due to the structure of the linear lattice and to the presence of nonlinear forces (sextupoles). We assume that the natural chromaticity, present in the linear lattice, is zero. In the case of a simple lattice with a single thin sextupole the tune shift due to the off momentum is given by [5]

$$\delta\omega_x = -\alpha\frac{p-p_s}{p_s} + O\Big(\,(\frac{p-p_s}{p_s})^2\,\Big), \qquad \alpha = k_2\beta\,D$$

where β and the dispersion D are evaluated at the sextupole position and k_2 is the sextupolar gradient. We propose the following model for the synchro-betatron coupling

$$\begin{pmatrix} j_{n+1} \\ \\ \theta_{n+1} \end{pmatrix} = \begin{pmatrix} j_n - \lambda\sin(2\pi\,h\,\theta_n) \\ \\ \theta_n + \eta\,j_{n+1} + \dfrac{\alpha}{2k_2^2\beta^3}\,f'(j_{n+1})\;\;(x_n^2 + (p_{x\,n} + x_n^2)^2) \end{pmatrix} \quad \mathrm{mod}\ 1$$

$$\begin{pmatrix} x_{n+1} \\ \\ p_{x\,n+1} \end{pmatrix} = R(\omega_x + \alpha\,f(j_{n+1}))\begin{pmatrix} x_n \\ \\ p_{x\,n} + x_n^2 \end{pmatrix} \tag{1}$$

where h is the harmonic number equal to the ratio between the RF frequency and the revolution frequency. The function $f(j)$ is periodic with period 1 and

such that $f(\jmath) = \jmath + O(\jmath^2)$. We choose $f(\jmath) = (2\pi)^{-1}\sin(2\pi\jmath)$ in all the numerical examples considered below; if $\lambda \ll 1$ the results are the same as for the linear function $f(j) = \jmath$. We have assumed that in our lattice there is only one RF cavity and a sextupole nearby. The constant λ is given by

$$\lambda = \frac{eV\,c^2}{E_s\,v_s^2}$$

where V is the maximum potential difference of the cavity, E_s is the energy of the synchronous particle whose velocity and momentum are v_s and p_s. If there are N cavities then $\eta \to \eta/N$. The x, p_x coordinates we use are scaled with respect to the normalized Courant Snyder coordinates $\hat{x}, \hat{p}_x$, and $\jmath, \theta$ are the normalized longitudinal momentum and phase defined by

$$x = \hat{x}\ k_2\,\beta^{3/2}, \quad p_x = \hat{p}_x\ k_2\,\beta^{3/2}, \qquad \jmath = \frac{p_s - p}{p_s} \equiv -\frac{\delta p}{p_s}, \quad \theta = \frac{\phi - \phi_s}{2\pi h} \equiv \frac{\delta\phi}{2\pi h} \tag{2}$$

where $\phi_s = 2\,\pi\,h\,n$ is the phase of the nearby synchronous particle after n turns, for which the potential jump $V\sin\phi$ across the cavity vanishes. For a realistic machine like SIS we have $\lambda \sim 10^{-3}$, $k_2 = 10^{-2}$ and $\eta \sim 1$, $h = 4$. Choosing $\beta = 10$, $D = 2$ we have $\alpha \sim 0.2$ and $\alpha/2k_2^2\beta^3 \sim 1$. In the mathematical model we consider the choice $2k_2^2\beta^3 = 1$ and $\eta = 1$ is made, leaving only λ and α as variable parameters.
Choosing $\alpha = 0$ this model reduces to the standard map and the Hénon map.
Letting $\delta\phi_n = \phi_n - \phi_s$ be the phase shift with respect to a synchronous particle and $\delta E_n = E_n - E_s$ be the energy shift, one has [6]

$$\begin{cases} \delta\phi_{n+1} = \delta\phi_n - 2\pi\,h\,\eta\dfrac{\delta p_{n+1}}{p_s} \\ \delta E_{n+1} = \delta E_n + eV(\sin\phi_n - \sin\phi_s) = \delta E_n + eV\sin\delta\phi_n \end{cases}$$

Using the kinematic identity

$$\frac{\delta p_n}{p_s} = \frac{c^2}{v_s^2}\,\frac{\delta E_n}{E_s}$$

and the normalized variables (2) we can write the map as

$$\begin{cases} \jmath_{n+1} = \jmath_n - \dfrac{eV\,c^2}{E_s\,v_s^2}\sin(2\pi h\theta_n) \\ \theta_{n+1} = \theta_n + \eta\jmath_{n+1} \end{cases} \tag{3}$$

On the other hand the Hénon map written in Courant Snyder coordinates reads

$$\begin{pmatrix} \hat{x}_{n+1} \\ \\ \hat{p}_{x\ n+1} \end{pmatrix} = R(\omega_x) \begin{pmatrix} \hat{x}_n \\ \\ \hat{p}_{x\ n} + k_2\,\beta^{3/2}\ \hat{x}_n^2 \end{pmatrix} \tag{4}$$

The coupling has been chosen so that the map is symplectic. More generally we replace the linear tune shift $\alpha\jmath$ with the derivative of $f(\jmath)$ where $f(\jmath+1) = f(\jmath) = \jmath + O(\jmath^2)$ so that the map is continuous on the torus. This is not relevant for beam physics but the map, extended to any value of $\jmath$, remains continuous and bounded. To prove that this map is symplectic we show that it is the Poincaré map of the following time periodic Hamiltonian

$$H = \frac{\omega}{2}(\hat{x}^2 + \hat{p}_x^2) + \eta\frac{\jmath^2}{2} + \alpha f(j)\ \frac{\hat{x}^2 + \hat{p}_x^2}{2} + \left(-\frac{\lambda}{2\pi h}\cos(2\pi h\,\theta) - k_2\beta^{3/2}\frac{\hat{x}^3}{3}\right)\delta_P(\sigma) \tag{5}$$

where $\delta_P(\sigma)$ is the periodic Dirac function of period 1 in $\sigma = s/L$, where L is the length of the FODO cell. Splitting H into $H_0 + H_1\delta_P(s)$ and introducing action and angles θ_x, j_x for the transverse motion we have

$$H_0 = \eta\frac{1}{2}\jmath^2 + \omega\ j_x + \alpha f(\jmath)\ j_x, \qquad j_x = \frac{\hat{x}^2 + \hat{p}_x^2}{2}$$

whose solution is given by

$$\theta(s) = \theta(0) + \left(\eta\jmath\ +\ \alpha f'(j)j_x\right)\ s, \qquad \theta_x(s) = \theta_x(0) + \left(\omega\ +\ \alpha f(\jmath)\right)\ s$$

The map from $s = n$ to $s = n+1$ of the unperturbed Hamiltonian immediately follows and composing it with the map corresponding to the impulsive contribution in Hamiltonian we obtain

$$\begin{pmatrix} \jmath_{n+1} \\ \theta_{n+1} \\ \hat{x}_{n+1} \\ \hat{p}_{x\ n+1} \end{pmatrix} = \begin{pmatrix} \jmath \\ \theta + \eta\, j + \alpha f'(\jmath)\,\dfrac{\hat{x}^2 + \hat{p}_x^2}{2} \\ \\ R(\omega_x + \alpha f(\jmath)) \end{pmatrix} \begin{pmatrix} \jmath_n - \lambda\sin(2\pi h\,\theta_n) \\ \theta_n \\ \hat{x}_n \\ \hat{p}_{x\ n} + k_2\beta^{3/2}\hat{x}_n^2 \end{pmatrix} \tag{6}$$

Written in explicit form the map (6) reads

$$\begin{pmatrix} j_{n+1} \\ \theta_{n+1} \end{pmatrix} = \begin{pmatrix} j_n - \lambda\sin(2\pi\ h\,\theta_n) \\ \theta_n + \eta\, j_{n+1} +\ f'(\jmath_{n+1})\ \dfrac{\alpha}{2}\,(\hat{x}_n^2 + (\hat{p}_{x\ n} + k_2\beta^{3/2}\ \hat{x}_n^2)^2) \end{pmatrix} \bmod 1$$

$$\begin{pmatrix} \hat{x}_{n+1} \\ \hat{p}_{x\ n+1} \end{pmatrix} = R\big(\omega_x + \alpha f(\jmath_{n+1})\big) \begin{pmatrix} \hat{x}_n \\ \hat{p}_{x\ n} + k_2\beta^{3/2}\ \hat{x}_n^2 \end{pmatrix} \tag{7}$$

Replacing $\hat{x}, \hat{p}_x$ with x, p_x according to (2) the map (1) is recovered.

ACTION-FREQUENCY MAP ANALYSIS

We have introduced the map (1) by coupling the transverse motion to the longitudinal motion by the chromatic effect of the sextupole, introduced as a shift in the linear frequency due to the off momentum. The coupling of the longitudinal motion to the transverse one was automatically fixed by the requirement that the map is symplectic. When the coupling vanishes the usual description of the longitudinal and transverse motion is recovered. The model enables us to see how the increase of the transverse emittance influences the change of the longitudinal momentum. We first analyze the dynamical features of the map (1), with $\eta = 1,\ 2k_2^2\,\beta^3 = 1,\ h = 1$, when the potential strength λ and the coupling α are varied in a physically reasonable interval. Dynamically the model is well defined even outside the bucket, namely the pendulum separatrix, and the restriction to the torus (by the mod 1 condition) makes the map bounded. If λ is large the map becomes chaotic and the model describes a random perturbation to the linear betatronic frequency is α is small. At $\lambda \simeq (2\pi)^{-1}$ the chaotic transition occurs since the last KAM curve is broken whereas for $\lambda \ll 0.1$ the map is a good integrator of the pendulum and the phase portrait is almost the same. When the coupling is switched on the phase plots show that the pendulum drive on the oscillator is significant and the reverse is even more important. In order to analyze the global aspects of the dynamics such as the location and strength of nonlinear resonances or the presence of chaotic regions it is convenient to have a two dimensional plot in frequency space or in action space, since the 2-dimensional or 3-dimensional projections do not allow to obtain a global view of the dynamics.

Analysis of 2D maps

We first describe the frequency analysis when the system is uncoupled. The frequency analysis for integrable systems is locally defined in every region delimited by a separatrix. For the Hénon map in the neighborhood of the origin, (almost all) the invariant curves are slightly distorted circles represented by

$$\begin{aligned} x &= (2a)^{1/2}\cos\phi, \qquad p_x = -(2a)^{1/2}\sin\phi \\ \phi &= \Theta + f(J,\Theta), \qquad a = J + g(J,\Theta), \end{aligned} \tag{8}$$

where $\Theta,\ J$ are the angle-action coordinates and $f,\ g$ are periodic functions. Expanding the invariant curves in a Fourier series we write

$$x - i\,p_x = \sum_k c_k(J) e^{ik\Theta} \tag{9}$$

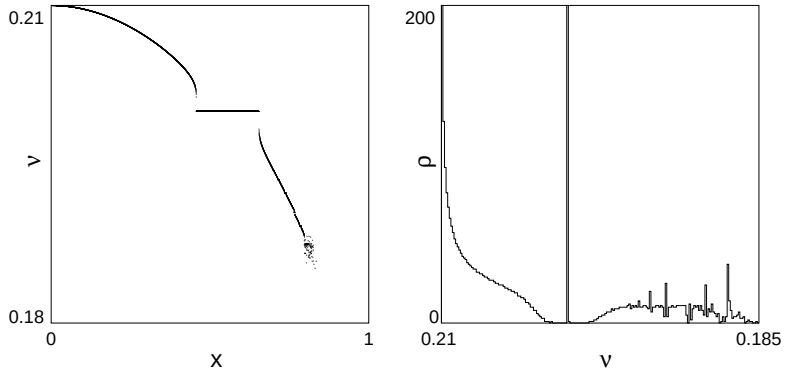

FIGURE 1. Frequency plots for the Hénon map on the line p_x=0 for linear frequencies $\omega/2\pi$=0.21. On the left is shown $\nu(x)$=$\Omega(x)/2\pi$, on the right the histogram of the frequency density $\rho(\nu)$

The orbits of the map with a non-resonant frequency are dense on a close curve and their Fourier representation is given by

$$x - i\,p_x = \sum_k c_k e^{ik(n\Omega(J)+\Theta(0))} \tag{10}$$

We choose the points uniformly distributed on a half line issued from the origin, for instance the positive x axis. The frequency of each orbit issued at the point $(x,0)$ is $\Omega = f(x)$ and the density of points in frequency space is

$$\rho(\Omega) = \rho_0 \sum_i \left|\frac{df}{dx}\right|^{-1}_{x_i}, \qquad f(x_i) = \Omega$$

If Ω is locked to a resonance Ω_* for $x_{\,\mathrm{min}} \le x \le x_{\,\mathrm{max}}$ then $f(x) \sim \Omega_* - |x - x_{\,\mathrm{min}}|^{1/\alpha}$ with $\alpha > 1$ for $x < x_{\,\mathrm{min}}$. The density $\rho(\Omega)$ vanishes as $(\Omega - \Omega_*)^{\alpha-1}$ by approaching Ω_*. There is an empty region around Ω_* and ρ diverges at Ω_*, see figure 1, where the tune $\nu(x) = \Omega/2\pi$ plot and the histogram $\rho(\nu)$ are shown. The action is given by

$$J = \frac{1}{2\pi}\oint p\,dq = \frac{1}{2\pi}\int_0^{2\pi} p(\Theta)\frac{\partial q}{\partial \Theta}\,d\Theta = \frac{1}{2}\sum_k k|c_k|^2 \tag{11}$$

and is defined at every point where Ω is non resonant. The map $\Omega(J)$ is known for every trajectory with non resonant Ω since the tracking points are dense on the closed orbit. For a resonance, the frequency Ω is locked and corresponding action interval is $[J_{\,\mathrm{min}}, J_{\,\mathrm{max}}]$ where the ends correspond to the actions of the inner and outer separatrix.

Defining J by the sum (11) over the resonant Fourier components we find that its value falls in the interval $[J_{\,\mathrm{min}}, J_{\,\mathrm{max}}]$, see figure 2. This is not surprising by

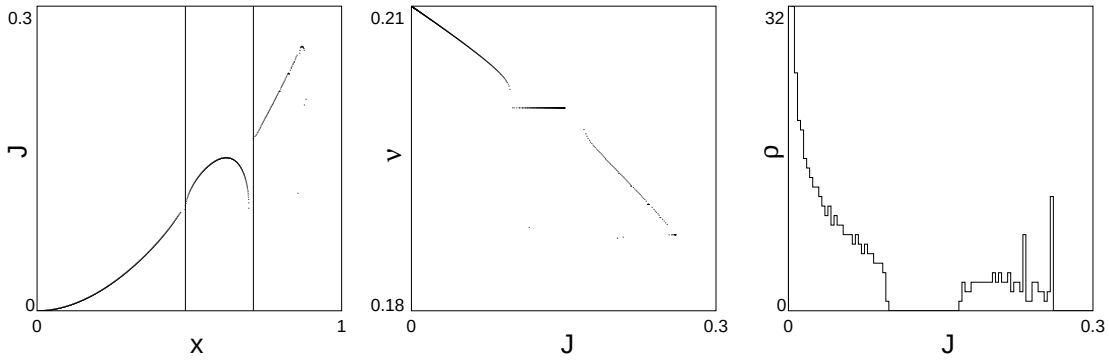

FIGURE 2. Action $J(x)$ of the Hénon map with linear frequency $\omega/2\pi$=0.21 for the points of the line p_x=0 (left), tune-action map $\nu(J)$ (center), action density $\rho(J)$ (right)

considering the interpolated orbit, which cannot reproduce the islands having to be connected but falls between the inner and the outer separatrix.
As a consequence the plot $\Omega(J)$ has holes where the frequency is locked and the width of the hole is the resonance width, see figure 2. The analysis extends to any 4D map.

DYNAMICAL FEATURES OF THE MODEL

We describe the dynamical behavior of the map (2.2) where $2k^2\beta^3 = 1$ and $h = 1$. The linear tune of the Hénon map is chosen to be $\omega_x/2\pi = 0.21$ so that the nonlinear tune decreases and locks on the resonance 5 as we move out from the origin. The chain of islands intersects the x axis on the interval $[0.45, 0.65]$ and the dynamic aperture is at $x = 0.8$. We have analyzed the 2D projections of the orbits for $\lambda = 0.001$ by varying the coupling from a very small $\alpha = 10^{-3}$ up to the physical value $\alpha = 10^{-1}$.
The normalized coordinates (x, p_x) were chosen in the interval $[-1, 1]$; since θ, j vary in the interval $[-1/2, 1/2]$, in order to have the same range in both phase planes we plot $(2\theta, 2j)$. The linear frequency of the standard map is $\omega_j/2\pi = (\lambda/2\pi)^{1/2} = 0.0126$ and the amplitude of the island corresponding to the pendulum oscillations is $\Delta j = 2(\lambda/2\pi)^{1/2} = 0.252$.

The figures 3 shows for $\alpha = 0.01$ the projection of the orbits in the x, p_x plane for two initial conditions in the other plane $j_0 = 0, 2\theta_0 = 0.1$, close to the elliptic fixed point, and $j_0 = 0$, $2\theta_0 = 0.99$ close to the hyperbolic fixed point. The projections in the θ, j phase plane are also shown for two distinct initial conditions $x_0 = 0.2, p_{x\,0} = 0$ close to the origin and $x_0 = 0.7, p_{x\,0} = 0$ close to the dynamic aperture.
The frequencies for all the orbits for initial conditions in the region $0 \leq x_0 \leq$

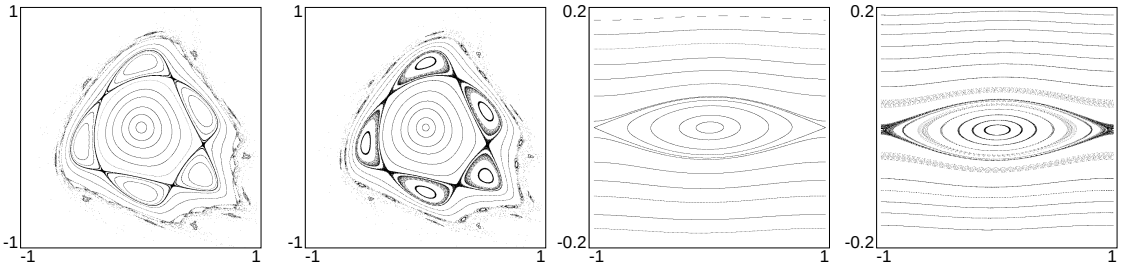

FIGURE 3. Phase plots of the Hénon map with $\omega_x/2\pi$=0.21, α=0.01, λ=0.001. Phase plane x,p_x with initial conditions: j_0=0, $2\theta_0$=0.1 (left), j_0=0, $2\theta_0$=0.99 (center left) Phase plane 2θ, $2j$ with initial conditions x_0=0.1, $p_{x\ 0}$=0 (center right), x_0=0.7, $p_{x\ 0}$=0 (right)

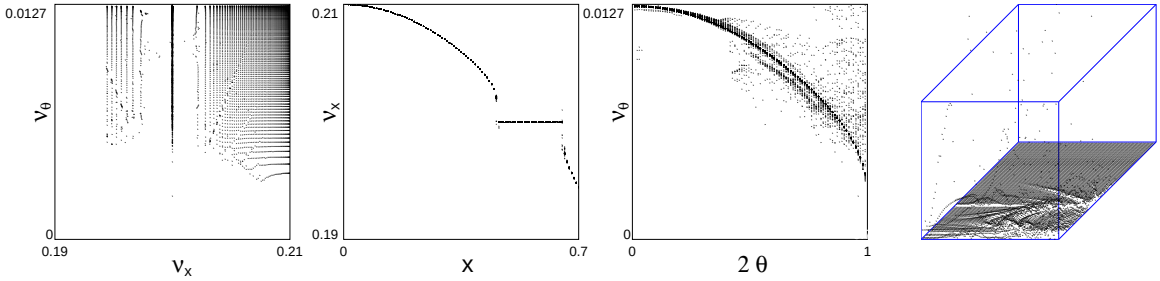

FIGURE 4. Frequency analysis for $\omega_x/2\pi$=0.21, α=0.01, λ=0.001. Plot in the ν_x, ν_θ plane (left), plot ν_x,x (center left), plot ν_θ versus 2θ (center right), error plot in the plane x, 2θ with a scale [0,0.01] (right)

0.7, $0 \leq 2\theta_0 \leq 0.99$ and $p_{x\ 0} = j_0 = 0$ have also been computed chosing a uniform grid of 100×100 and 2000 iterations for each initial condition (the 600 MH CPU time is 1 minute since only one harmonic is evaluated). The results are shown in the figures 4. For a very weak coupling $\alpha = 0.001$ the projection of the orbits in the x, p_x plane is almost unaffected, whereas in the θ, j plane a deformation is visible when the initial condition in the (x, p_x) plane is chosen inside the islands. For the intermediate coupling $\alpha = 0.01$, see figure 3, the chaotic layers near the separatrices in both planes are well visible. The width of the layer in the x, p_x plane is the largest for initial conditions close to the separatrix in the $(\theta,\ j)$ plane. The width of the chaotic layer in the $(\theta,\ j)$ plane becomes significant when we cross the island and approach the dynamic aperture in the (x, p_x) plane. We show also an error plot of the Fourier reconstruction of the orbit: points with large errors are scattered and correspond to chaotic orbits.

We have also considered another example with a linear frequency $\omega_x/2\pi = 0.175$ and $\lambda = 0.18$, above the critical value $\lambda_c \simeq (2\pi)^{-1}$. In this case the linear frequencies are comparable since $\omega_j/2\pi = 0.178$; the coupled $1:1$ resonance and many others appear. Since λ is large, the map is a bad integrator of the pendu-

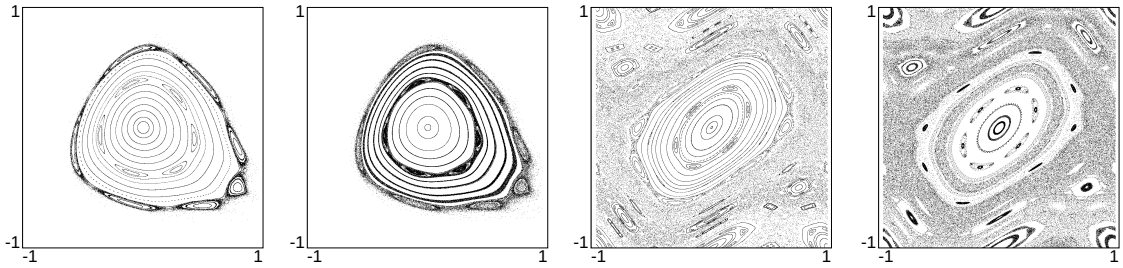

FIGURE 5. Phase plots for =0.175, α=0.01, λ=0.18. Phase plane x,p_x with initial conditions: J_0=0, $2\theta_0$=0.1 (left), J_0=0,$2\theta_0$=0.99 (center left) Phase plane 2θ, $2J$ with initial conditions x_0=0.1, $p_{x\ 0}$=0 (center right), x_0=0.7, $p_{x\ 0}$=0 (right)

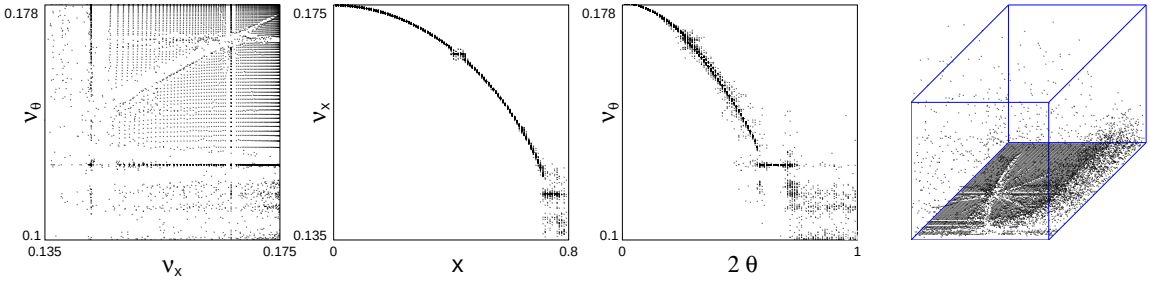

FIGURE 6. Frequency analysis for $\omega_x/2\pi$=0.175, α=0.01, λ=0.18. Plot in the ν_x, ν_θ plane (left), plot ν_x,x (center left), plot ν_θ,2θ (center left), error plot in the plane x,2θ with a scale [0,0.1] (right)

lum, whose linear tune $(\lambda/2\pi)^{1/2} = 0.169$ differs from $\omega_j/2\pi$. The separatrix is replaced by large stochastic layer and initial conditions there produce a random perturbation of the linear frequency of Hénon map, see figures 5. Many resonant structures are visible as confirmed by the frequency analysis, see figure 6.

A physical example

We have considered the mapping (1) for a set of the parameters compatible with SIS namely $k_2 = 0.01$, $\beta = 10, D = 1$ so that $\alpha = 0.1$ and the coefficient $(2k_2^2\beta^2)^{-1}$ which multiplies the coupling term in the longitudinal plane is equal to 5 rather than to 1, the value chosen in the previous examples. For comparison we have condered first a case where the dispersion is very small $D = 0.1$ so that $\alpha = 0.01$. The dynamic aperture in the normalized variables is $A = 0.6$ along the x axis.

In the weakly coupled case $\alpha = 0.01$ as long as we remain up to 1/6 the dynamic aperture, the coupling effect is negligible in the longitunal cordinates; the effect becomes apreciable at 1/2 of the dynamic aperture and has a strong randomizing effect close to the dynamic aperture. Due to the absence of resonances of appre-

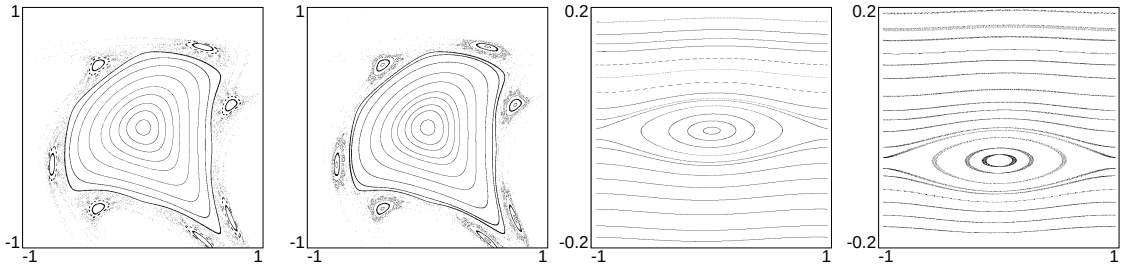

FIGURE 7. Phase plots for $\omega_x/2\pi$=0.295, α=0.1, λ=0.001. Phase plane x,p_x with initial conditions: j_0=0, $2\theta_0$=0.1 (left), j=0, 2θ=0.99 (center left) Phase plane θ, j with initial conditions x_0=0.1, $p_{x\ 0}$=0 (center right), x_0=0.3, $p_{x\ 0}$=0 (right)

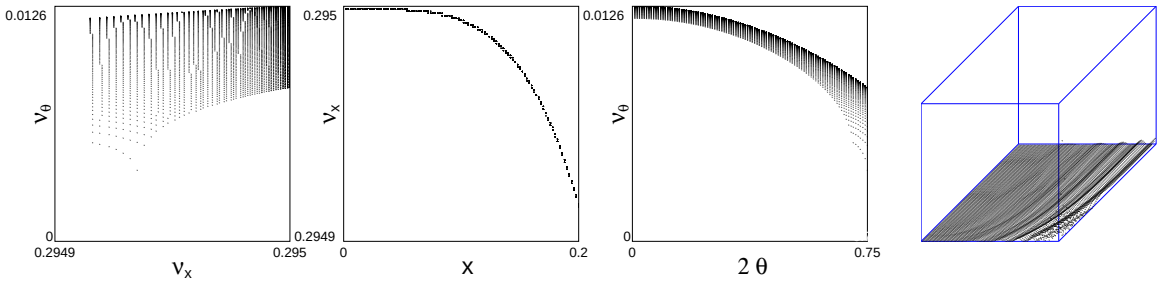

FIGURE 8. Frequency analysis for $\omega_x/2\pi$=0.295, α=0.1, λ=0.001. Plot in the ν_x, ν_θ plane with initial conditions restricted to $0<x_0<0.2$, $|2\theta_0|<0.75$ for (left), plot ν_x,x (center left), plot ν_θ,2θ (center left), error plot in the plane x,2θ (right) with a scale [0,0.0001]

ciable width the effect of coupling in the transverse plane is small, also when we are close the separatrix in the longitudinal phase plane (this is partly due to the factor $(2k_2^2\beta^2)^{-1}$ which is larger than 1 and enhances the coupling effect in the longitudinal phase plane).

For strong coupling $\alpha = 0.1$ below 1/6 of the dynamic aperture, namely for $p_{x\ 0} = 0, 0 < x_0 < 0.1$, the orbits in the longitudinal phase plane are weakly affected at least for initial conditions $0 < 2\theta_0 < 0.9$, $j_0 = 0$, see figure 7. Up to 1/3 of the dynamic aperture namely $p_{x\ 0} = 0, 0 < x_0 < 0.2$ the longitudinal orbits are still regular at least for $0 < 2\theta_0 < .75$, $j_0 = 0$. Approaching the dynamic aperture the longitudinal motion becomes very chaotic and the fixed point is displaced. In Figure 8 we show the frequency plots for initial conditions in the range $0 < x_0 < 0.2$, $p_{x\ 0} = 0$ and $0 < 2\theta_0 < .75$, $j_0 = 0$. Approaching the dynamic aperture the longitudinal motion becomes very chaotic.

Action frequency map and resonances

In order to have a better understanding of the dynamics when it is more intricate we have carried a more refined frequency analysis choosing a 600×600 grid and

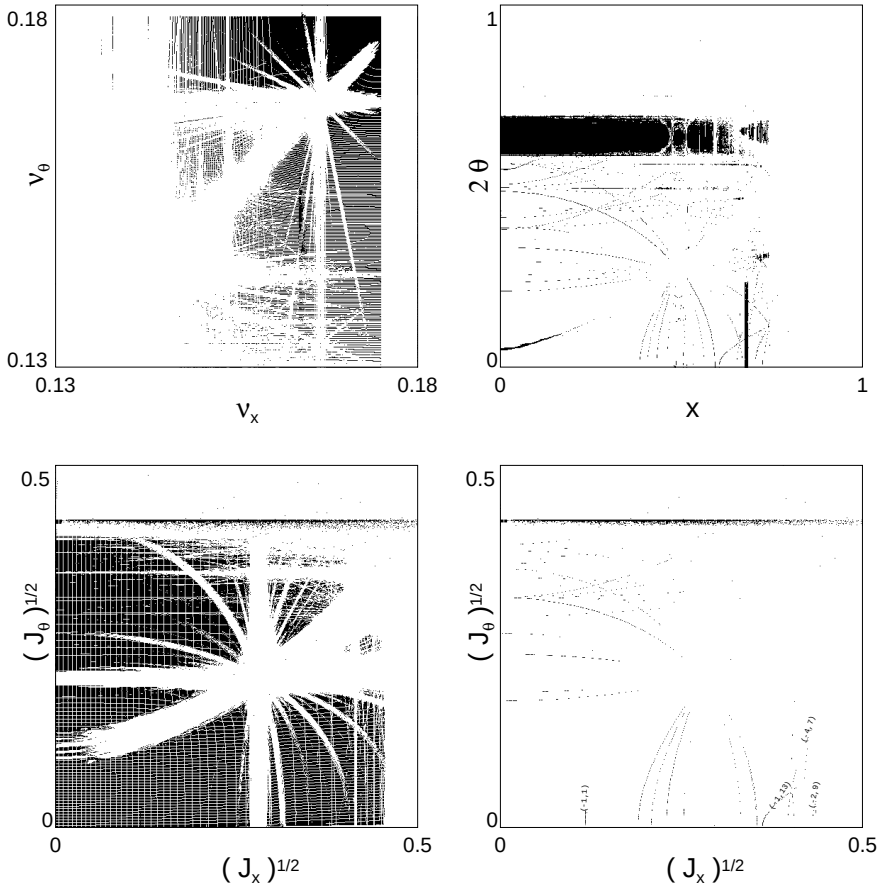

FIGURE 9. Frequency analysis for $\omega_x/2\pi$=0.175 α=0.01, λ=0.18. Plot in the ν_x, ν_θ plane of the points with a discrepancy less than 0.01 (upper left). Resonance lines in the x,2θ plane (upper right). Plot of nonresonat tori in the actions plane ($\sqrt{J_x}$, $\sqrt{J_\theta}$ (lower left). Resonance lines in the actions plane ($\sqrt{J_x}$, $\sqrt{J_\theta}$ (lower right)

evaluating the harmonics up to order 10 (600 MH CPU time $\sim$ 7 hours). We have chosen $\omega_x/2\pi = 0.175$ and $\lambda = 0.18$ and $\alpha = 0.01$. The frequency plot ν_x, ν_θ, see figure 9 is obtained by dropping the points where the mean discrepancy between the signal and its reconstruction is larger than 0.01. A resonance plot consists of all the points in the $x, 2\theta$ plane whose orbits are resonant.
The actions for all the nonresonant orbits have been evaluated. In the actions space $J_x^{1/2}$, $J_\theta^{1/2}$ we plot all the points which correspond to the non resonant orbits. The resonances in this plot are empty channels. Finally we have also determined the values of the action given by the algorithm (11) within the resonances (excluding the 1:1). The lines so obtained fall within the empty channels of the previous plot and are close to the resonance lines in the $x, 2\theta$ plane, as one should expect close to the stable elliptic point from normal form theory [7].

CONCLUSIONS

To summarize the proposed model seems adequate to describe the synchro-betatron coupling. As we should expect far enough from the dynamic aperture the coupling effect is small and the longitudinal motion is scarcely affected. By increasing the transverse amplitude, the longitudinal orbits are distorted and then become chaotic. The frequency analysis proves to be useful to determine the safety regions. The longitudinal motion affects the transverse one when resonances are present. In this case the islands become chaotic especially when the initial condition are chosen close to the separatrix in the longitudinal phase plane. The diffusion process can be analyzed in this case following well established techniques. From the dynamical point of view the model is rich and allows to explore different regimes. For instance when λ approaches the critical value $\lambda = 1/2\pi$ the linear frequencies become comparable and many coupled resonances appear as for coupled Hénon maps. A large stochastic layer appears in this case and for initial conditions there the transverse motion is almost the same as for a random perturbation of the linear betatronic frequency. This model can be used also to explore how a random perturbation in the longitudinal coordinates determines a diffusion of the emittance.

ACKNOWLEDGMENTS

We are indebted to Dr. Bazzani for discussions on the frequency analysis.

REFERENCES

[1] M. Prome *Proceedings of the 1996 International Linac Conference*, Geneva, CERN 96-07, p.9 (1996)

[2] H. I. Hofmann, Proceedings of EPAC, Stiges 10-14 June, Institute of Physics Publishing, Bristol, p. 225. (1996)

[3] M. Giovannozzi, W. Scandale, E. Todesco Part. Accel. **56**, 195 (1997)

[4] M. Fisher, M. Giovannozzi, F. Schmidt Phys. Rev. **E 55**, 3507 (1997)

[5] G. Franchetti, G. Turchetti *The micromaps description of a beam with space charge*, Proceedings of the Workshop "Nonlinear and Collective Phenomena in Beam Physics" Arcidosso 1-4 September 1996, this volume.

[6] G. Dome *Theory of RF acceleration* CAS Cern Accelerator School 1985, E. S. Turner, CERN 87-03 (1987)

[7] A. Bazzani, E. Todesco, G. Turchetti, G. Servizi *A normal form approach to the theory of nonlinear betatronic motion* CERN Yellow Report 94-02 (1994)